Research in Astronomy and Astrophysics, 25:105012 (7pp), 2025 October
https://doi.org/10.1088/1674-4527/adf9db
CSTR: 32081.14.RAA.adf9db
© 2025. National Astronomical Observatories, CAS and IOP Publishing Ltd. All rights, including for text and data mining, AI training, and similar technologies, are reserved.

The Role of the Disk Magnetization in the Production of Jets

Hamed Marzougui and Mouna Khlifi
Laboratory of Soft Matter Physics and Fluid Physics, Department of Physics, Faculty of Sciences, El Manar, 2092, Tunis, Tunisia; hamed.marzougui@ipeiem.utm.tn
Received 2025 February 12; revised 2025 July 29; accepted 2025 August 8; published 2025 September 9

Abstract

In this paper, we present results from a semi-analytical model that investigates the launching of cold, non-relativistic jets from a wide radial extent of stationary and axisymmetric magnetized accretion disks. Specifically, we examine the effects of magnetization on the disk-jet system in configurations where the magnetic field is near equipartition with the thermal pressure at the disk midplane. In this study, the magnetic strength parameter μ is explicitly expressed as a function of the magnetic diffusivity parameter α_m ($\mu \sim 1/\sqrt{\alpha_m}$). This formulation provides a more direct link between the magnetic field configuration and the diffusive processes within the accretion disk. By establishing this relationship, we better constrain the role of magnetization in jet launching and explore how variations in μ influence the overall disk-jet dynamics. We focus on three representative cases where μ takes the values 0.5, 0.7, and 0.9. We solve the stiff ordinary differential equations of the semi-analytical MHD model using the Seulex subroutine of Hairer & Wanner, which employs the Taylor method with adaptive mesh refinement. The resulting solutions are compared with those obtained by Zanni et al., Tzeferacos et al., and Stepanovs & Fendt.

Key words: accretion disks – magnetohydrodynamics (MHD) – turbulence – ISM: jets and outflows

1. Introduction

Astrophysical jets have been observed in various contexts, including young stellar objects, relativistic stars, galactic objects and active galactic nuclei. These jets extend over distances of approximately 5 pc from their launching region. Typically, they are bipolar, highly collimated and exhibit velocities ranging from 200 km s^{-1} for low-mass young stellar objects to relativistic speeds for active galactic nuclei.

Despite their differences in spatial, temporal, and energy scales, it is widely accepted by the astrophysical community that jets are launched from accretion disks composed of ionized matter surrounding central objects. These disks are threaded by large-scale magnetic fields of bipolar topology. Such magnetic fields extract energy and angular momentum from the disks, allowing accretion to proceed while accelerating a fraction of the disk matter so that it can escape the gravitational potential well of the central object.

Numerous studies have been conducted to understand the mechanisms responsible for the jet launching, acceleration and collimation. Blandford & Payne (1982) proposed a magneto-centrifugal MHD model in which a magnetized jet is launched from a Keplerian disk and accelerated in opposite directions along the disk's axis by a Poynting flux generated at the disk's surface. Their model demonstrated that jets are produced when the poloidal component of the magnetic field exists at an angle greater than 30° relative to the disk's rotation axis. The idea introduced by Blandford & Payne (1982) is of the origin of numerous time dependent numerical simulations and steady state models. The first numerical simulations investigating time-dependent jet solutions, treating the disk as a boundary condition, date back to the works of Ustyugova et al. (1999), Ouyed & Pudritz (1997), Krasnopolsky et al. (1999), Anderson et al. (2005), Fendt (2006), Pudritz et al. (2006). These simulations provide steady solutions over short timescales; therefore they do not fully capture the acceleration and collimation processes because they neglect the back-reaction of the jet on the disk.

Observational correlations between accretion and ejection signatures in jet sources, as detected by Cabrit et al. (1990), provide clear evidence of the interdependence between these processes. This suggests that the disk and jet must be studied together as part of a so-called accretion-ejection structure. Numerical simulations of the entire disk-jet system have been developed by Uchida & Shibata (1985) and Kato et al. (2002). However, these simulations break down under the assumption of an ideal MHD disk, leading to highly unstable outflows over short simulated timescales. This instability results from the extreme advection of magnetic field lines by accreting matter onto the central object, producing a strong magnetic torque that removes excessive angular momentum, ultimately suppressing the disk. This phenomenon, known as the magnetic braking catastrophe in the ideal MHD limit, was identified by Tomisaka (2000), Allen et al. (1995) and Mellon & Li (2008).

Non-ideal MHD effects due to viscosity and magnetic diffusivity were first included in disks by Ferreira & Pelletier (1995), Ferreira (1997) and Casse & Ferreira (2000). To

balance the shearing caused by differential rotation and the advection of field lines by the accretion of matter onto the central object, they proposed that transport coefficients (viscosity and magnetic diffusivity) must arise from turbulent processes. Turbulence in the disk is usually generated by various unstable modes, such as magneto-rotational instability in moderately magnetized disks and Parker instability for stronger magnetized disks. In their steady-state semi-analytical models, Ferreira & Pelletier (1995) and Casse & Ferreira (2000) adopted the assumption that jets are cold, meaning that enthalpy does not significantly contribute to the accretion-ejection dynamics. Based on this assumption, they concluded that such jets occur when the thermal energy is in equipartition with magnetic energy inside the disk and the poloidal thermal pressure gradient is the only force driving disk matter into jets.

Time-dependent numerical simulations of jet production from purely magnetized accretion disks date back to the serious works of Casse & Keppens (2002), Casse & Keppens (2004) published in two separate papers referred to as CK02 and CK04, respectively. In CK02, they studied cold jets launched from a weakly diffusive magnetized disk in a near-equipartition state ($B^2/2\mu_0 P = 0.6$). In CK04, they explored warm jets using the same initial parameters as in CK02. In both studies, their simulations achieved a near-stationary state of magnetized accretion disks launching superfast magneto-sonic jets within relatively short timescales corresponding to 0.13 rotation periods at the outer radius $r = 40$. The fraction of matter carried away by jets was found to be roughly 15% of the accretion rate for cold jets and 22% for warm jets.

The magnetization effects on accretion-ejection structures have been widely studied by Tzeferacos et al. (2009), Murphy et al. (2010), Sheikhnezami et al. (2012), Stepanovs & Fendt (2014) and Stepanovs & Fendt (2016). Time dependent numerical simulations of Tzeferacos et al. (2009) for purely magnetized disks confirmed the findings of Ferreira & Pelletier (1995), Casse & Keppens (2002), Casse & Keppens (2004) suggesting that only an accretion disk in equipartition can produce fast magnetosonic jets. Including the effects of viscosity, Murphy et al. (2010), Rezgui et al. (2019) and Rezgui et al. (2022) showed that fast magnetosonic jets can also be produced by weakly magnetized disks. Sheikhnezami et al. (2012) concluded that the driving mechanism of such jets is not governed by the magneto-centrifugal acceleration of Blandford & Payne (1982) but rather by magnetic pressure acceleration. Unlike Zanni et al. (2007), Tzeferacos et al. (2009), who treated diffusivity α_m and disk magnetization μ as independent parameters, Stepanovs & Fendt (2014) and Stepanovs & Fendt (2016) showed that these two parameters are closely linked: a decrease in α_m leads to an increase in μ.

The present work investigates the effects of magnetization on jet production from magnetized accretion disks. The magnetic strength parameter μ is expressed here as a function of the magnetic diffusivity coefficient α_m. The obtained results are qualitatively compared with those of Zanni et al, Tzeferacos et al. and Stepanovs & Fendt.

2. MHD Model for Non-ideal Accretion-ejection Disk

2.1. Non-relativistic MHD Equations

In the standard non-relativistic form, the MHD equations for a Debye plasma, under the single-fluid approximation, consist of the basic laws of mass, momentum and energy together with the induction equation for the magnetic field. These equations are:

$$\frac{\partial \rho}{\partial t} + \nabla \cdot (\rho u) = 0, \tag{1}$$

$$\rho \frac{\partial \boldsymbol{u}}{\partial t} + \rho(\boldsymbol{u} \cdot \nabla)\boldsymbol{u} = -\nabla P + \rho \boldsymbol{g} + \boldsymbol{J} \times \boldsymbol{B} + \nabla . \boldsymbol{T}, \tag{2}$$

$$\frac{\partial e}{\partial t} + \nabla \cdot [(e + P + \frac{\boldsymbol{B}\cdot\boldsymbol{B}}{2})\boldsymbol{u} - (\boldsymbol{u} \cdot \boldsymbol{B})\boldsymbol{B} + \bar{\bar{\eta}}_m \boldsymbol{J} \times \boldsymbol{B}] - \nabla \cdot (\boldsymbol{u} \cdot \boldsymbol{T}) = -\Lambda_{\rm cool}, \tag{3}$$

$$\frac{\partial \boldsymbol{B}}{\partial t} = \nabla \times [\boldsymbol{u} \times \boldsymbol{B} - \bar{\bar{\eta}}_m \nabla \times \boldsymbol{B}], \tag{4}$$

where ρ is the mass density, $\boldsymbol{u}$ the velocity field, P the plasma thermal pressure, $\boldsymbol{B}$ the magnetic field, $\boldsymbol{g}$ the gravitational field of the central object, $\boldsymbol{J} = \boldsymbol{\nabla} \times \mathbf{B}$ the current density, e the total energy density, $\bar{\bar{\eta}}_m$ the magnetic diffusivity tensor, $\boldsymbol{T}$ the viscous stress tensor and $\Lambda_{\rm cool}$ the cooling term mainly associated with the radiative losses.

2.2. Model Description

In this section, we describe the MHD model for a non-ideal disk driving an ideal cold jet. This model assumes a stationary, axisymmetric and geometrically thin non-ideal disk that rotates at a sub-Keplerian velocity around the central object. The disk is threaded by a large-scale open magnetic field with even symmetry, such that $B_r = B_\theta = 0$ at the disk midplane. It is important to note that in the cold jet approximation, the energy equation is replaced by the isothermality assumption of the magnetic surfaces given by $P = \rho c_s^2$, where c_s is the isothermal sound speed.

Using cylindrical coordinates, the MHD Equations (1) and (2), applied to a non-ideal accretion-ejection disk under the aforementioned assumptions, yield:

$$\frac{1}{r}\frac{\partial}{\partial r}(r\rho u_r) + \frac{\partial}{\partial z}(\rho u_z) = 0, \tag{5}$$

$$\rho u_r \frac{\partial u_r}{\partial r} + \rho u_z \frac{\partial u_r}{\partial z} = \rho g_r - c_s^2 \frac{\partial \rho}{\partial r} + \rho \frac{u_\theta^2}{r} + \frac{B_z}{\mu_0}\frac{\partial B_r}{\partial z} - \frac{1}{2\mu_0}\frac{\partial B_z^2}{\partial r} - \frac{1}{2r^2\mu_0}\frac{\partial (rB_\theta)^2}{\partial r} + (\boldsymbol{\nabla} \cdot \boldsymbol{T})_r, \tag{6}$$

$$\rho u_r \frac{\partial u_z}{\partial r} + \rho u_z \frac{\partial u_z}{\partial z} = \rho g_z - c_s^2 \frac{\partial \rho}{\partial z} + \frac{B_r}{\mu_0}\frac{\partial B_z}{\partial r} - \frac{1}{2\mu_0}\frac{\partial}{\partial z}(B_r^2 + B_\phi^2) + (\boldsymbol{\nabla}\cdot\boldsymbol{T})_z, \quad (7)$$

$$\frac{\rho u_r}{r}\frac{\partial}{\partial r}(r u_\theta) + \rho u_z \frac{\partial}{\partial z}(r u_\theta) = \frac{B_r}{r\mu_0}\frac{\partial}{\partial r}(rB_\theta) + \frac{B_z}{\mu_0}\frac{\partial B_\theta}{\partial z} + (\boldsymbol{\nabla}\cdot\boldsymbol{T})_\theta. \quad (8)$$

To achieve closure of these equations, we need to express the components of the magnetic field and the viscous stress tensor $\boldsymbol{T}$ in terms of known quantities. The components (B_r, B_z) of the poloidal magnetic field B_p are determined using the magnetic flux function Ψ

$$B_r = -\frac{1}{r}\frac{\partial \Psi}{\partial z},\ B_z = \frac{1}{r}\frac{\partial \Psi}{\partial r}, \quad (9)$$

where the Ψ function is the solution of Ohm's law equation

$$\Delta\Psi = \frac{\mu_0}{\eta_m^p}\left[u_z\frac{\partial \Psi}{\partial z} + u_r\frac{\partial \Psi}{\partial r}\right]. \quad (10)$$

The toroidal component B_θ is determined using the toroidal field induction

$$\nabla\cdot\left(\frac{\eta_m^t}{\mu_0 r^2}\nabla\ rB_\phi\right) = \nabla\ \cdot\frac{1}{r}(B_\theta \boldsymbol{u_p} - \boldsymbol{B_p} u_\theta). \quad (11)$$

In an axisymmetric disk dominated by rotational motion around a central object, only the toroidal component of the viscous stress tensor significantly impacts the accretion-ejection mechanism ($(\nabla\cdot\boldsymbol{T})_r = (\nabla\cdot\boldsymbol{T})_z = 0$). Therefore, the viscous force is reduced to a viscous torque given by

$$(\nabla\ \cdot\boldsymbol{T})_\theta = \frac{1}{r}\frac{\partial}{\partial r}\left(\rho\nu_\nu r^3\frac{\partial\Omega}{\partial r}\right), \quad (12)$$

where η_m^p, η_m^t, ν_ν and Ω are respectively the poloidal magnetic diffusivity, the toroidal magnetic diffusivity, the kinematic viscosity and the rotation rate. As previously mentioned, the kinematic viscosity and the magnetic diffusivity have a turbulent origin. In the present work, we apply the α-turbulent model of Shakura & Sunyaev (1973) which assumes that ν_ν at the disk midplane is proportional to the thermal heightscale h and the sound speed c_s

$$\nu_\nu(z=0) = \frac{2}{3}\alpha_\nu c_s h. \quad (13)$$

In previous studies, Casse & Keppens (2004), Zanni et al. (2007), Sheikhnezami et al. (2012), Stepanovs & Fendt (2014), Stepanovs & Fendt (2016) assumed that the magnetic diffusivity tensor is diagonal with the non-zero components, $\eta_{\theta\theta} = \eta_m^p$; $\eta_{rr} = \eta_{zz} = \eta_m^t$. By analogy with the α-prescription attributed by Shakura & Sunyaev to the kinematic viscosity, they proposed the following expression for the poloidal magnetic diffusivity at the disk midplane

$$\eta_m^p(z=0) = \alpha_m v_{\rm A}|_{z=0} h, \quad (14)$$

where $v_{\rm A}$ is the Alfvén speed and α_m is a constant parameter measuring the MHD turbulence intensity in the disk midplane.

The toroidal component η_m^t is assumed to be proportional to η_m^p through the anisotropy parameter $\chi_m = \eta_m^t/\eta_m^p$. In the dense disk connected to a dilute jet, the anomalous transport coefficients must be zero outside the disk. To achieve this, vertical profiles are imposed on these coefficients. Thus

$$\nu_\nu(r,z) = \nu_\nu(z=0) f_\nu(r,z);\ \eta_m^p(r,z) = \eta_m^p(z=0) f_m(r,z). \quad (15)$$

For the functions f_ν and f_m, several options can be considered. In the present work we apply the Gaussian form

$$f_\nu(r,z) = f_m(r,z) = exp(-z^2/h^2). \quad (16)$$

3. Numerical Method and Model Parameters

The ordinary differential Equations (5), (6), (7), (8), (10) and (11) governing the disk-jet system are solved using a method based on separable variables, assuming radial self similarity. With this assumption, all physical quantities $U(r,z) = (\rho, u_r, u_z, u_\theta, p, \Psi, B_\theta)$ in the above equations scale as the product of a power law in r with a function of the variable $x = z/h$,

$$U(r,z) = U_0\left(\frac{r}{r_0}\right)^{\alpha_u} F_u(x). \quad (17)$$

Here U_0 is the value of $U(r,z)$ at the disk midplane $(z=0)$ and at $r = r_0$. F_u is an even function such that $F_u(x=0) = 1$ or an odd function such that $F_u(x=0) = 0$, depending on the symmetry of the variable with respect to the midplane of the disk.

Self similarity requires that the sound speed c_s and the Alfvén speed $v_{\rm A}$ scale as the Keplerian velocity $v_k \sim r^{-1/2}$. With this method, we obtain two systems of equations: the first is an algebraic system whose unknowns are the power-law coefficients α_u, which describe the radial structure of disk-jet system. The solutions of this system are determined according to the β power law coefficient of the magnetic flux function as follows

$$\alpha_{u_r} = \alpha_{u_z} = \alpha_{u_\theta} = -1/2;\ \alpha_p = 2\beta - 4,$$
$$\alpha_\rho = 2\beta - 3;\ \alpha_{B_\theta} = \beta - 1.$$

In the present work, we apply the value of 0.77 for β given by Blandford & Payne (1982).

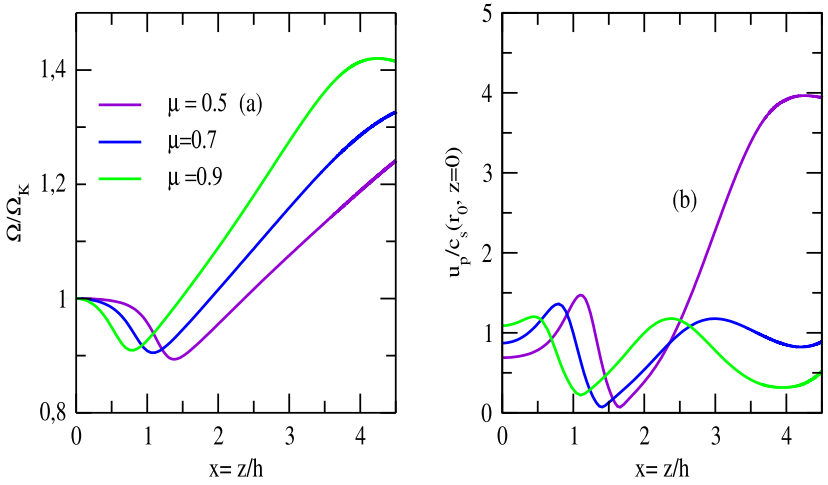


Figure 1. Spatial evolution of (a): angular velocity; (b): poloidal velocities.

The second system, which describes the vertical structure of disk-jet, consists of a set of ordinary differential equations for the functions F_u. These equations are solved from the disk-midplane up to $x = 6$, using the subroutine Seulex of Hairer & Wanner (1996). This system involves a total of five non-dimensional parameters:

(i) $\epsilon = \frac{h}{r}$, the disk geometrical thickness;

(ii) α_m, the magnetic diffusivity parameter;

(iii) $\chi_m = \frac{\eta_m^t}{\eta_m^p}$, the anisotropy parameter;

(iv) $\mu = \frac{v_A^2}{c_s^2} \sim 1/\sqrt{\alpha_m}$, the strength of the magnetic field;

(v) $\mathcal{P}_m = \frac{2}{3}\frac{\alpha_v}{\alpha_m}\mu^{1/2}$, the magnetic Prandlt number.

In the present work, we consider a magnetized accretion disk with geometric thickness of $\epsilon = 0.1$, where the magnetic field strength is near equipartition with the gas pressure. Thus, we choose values of μ equal to 0.5, 0.7 and 0.9. The magnetic diffusivity parameter is evaluated using the relation: $\mu = 1/\sqrt{\alpha_m}$. This relation is obtained from a refined analysis and interpolation of the results reported by Stepanovs & Fendt (2014). In the present study, we adopt $\chi_m = 0.5$ and $\mathcal{P}_m = 3/2$ as representative values of the anisotropy parameter and the magnetic Prandtl number, respectively.

4. Results and Discussion

Figure 1(a) and (b) shows the evolution curves of the angular and poloidal velocities of the matter in the disk-jet system as functions of $x = z/h$. Two distinct regions can be identified in these figures: the resistive region (MHD accretion disk) and the ideal MHD region (jet). Significant differences can be observed between the three cases with $\mu = 0.5$, 0.7, and 0.9: the transition from the resistive to the ideal region depends on the magnetization μ, or equivalently, on the magnetic diffusivity coefficient α_m, since $\mu = 1/\sqrt{\alpha_m}$. This behavior is also reported in the work of Ferreira (1997), who shows that the transition occurs on a height scale proportional to $\sqrt{\chi_m \alpha_m^2}$. In agreement with our results, we find that for a fixed value of χ_m, this transition occurs at a higher $z\ /\ h$ when the disk magnetization μ is decreased. Physically, a lower magnetization implies a weaker coupling between the magnetic field and the matter, requiring a larger distance from the midplane for the magnetic field to dominate and for ideal MHD conditions to be established.

Figure 1(a) shows that, within the disk, the angular velocity decreases as the magnetization parameter μ increases. We will see that this decrease is caused by a magnetic torque that slows down the disk and enables gravity to accrete matter onto the central object. Therefore, the magnitude of this torque must increase as μ increases. In contrast to the results reported by Tzeferacos et al. (2009), the resistive region in Figure 1(b) shows that magnetization leads to an increase in the accretion velocity. In the ideal MHD region (Figure 1(a)), the jet material undergoes azimuthal acceleration that intensifies with increasing μ. This behavior indicates that the magnetic torque, while acting to slow the disk, reverses sign at the disk surface and subsequently functions as a magnetic accelerator for the jet in the azimuthal direction. Figure 1(b) shows that the jet matter undergoes poloidal acceleration, driven by the conversion of Poynting flux into kinetic energy during propagation. Additionally, it indicates that efficient poloidal acceleration is favored in low-magnetization configurations.

Figure 2(a) and (b) shows the variation in the inclination of the poloidal magnetic field relative to the rotation axis of the central object and the poloidal velocity of the jet. These figures indicate that the current model satisfies the Blandford & Payne (1982) criterion, which states that for a cold jet, the angle between the poloidal magnetic field and the rotation axis of the central object at the disk surface must be greater than 30° to

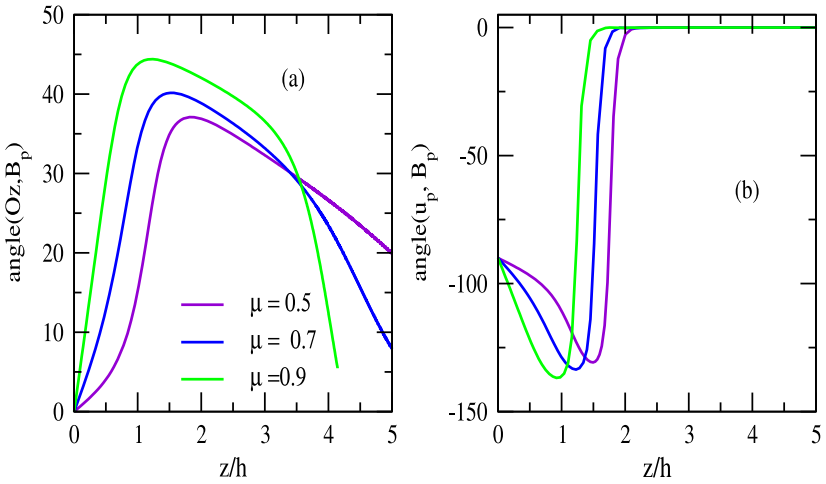


Figure 2. Spatial evolution of (a): angle between poloidal magnetic field and disk rotation axis; (b): angle between poloidal velocity and poloidal magnetic field.

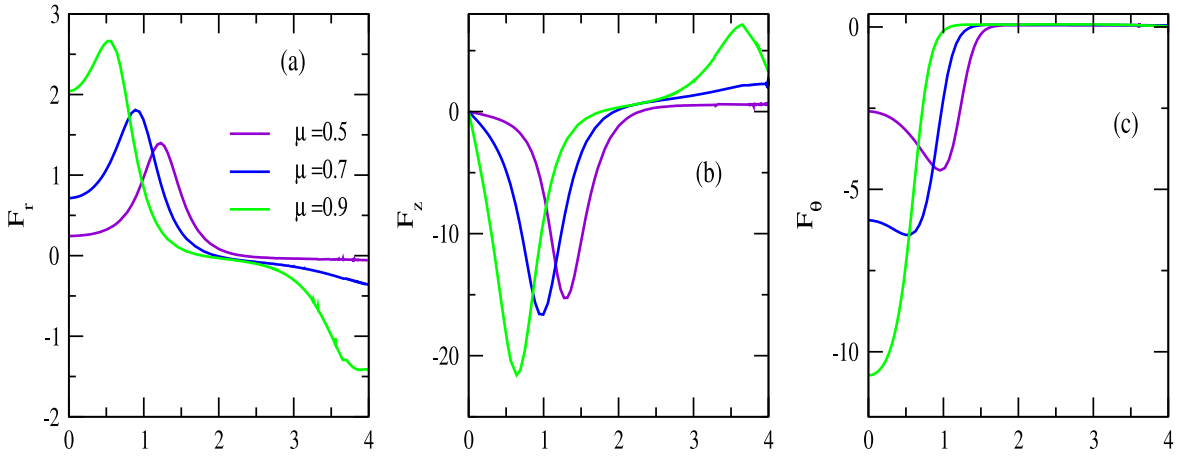


Figure 3. Spatial evolution of F_r (a), F_z (b) and F_θ (c) components of the magnetic force.

allow matter to be ejected. The model also satisfies the freezing-in condition, which requires that the poloidal velocity of the jet be parallel to the poloidal magnetic field, ensuring that jet matter remains frozen to the magnetic surfaces.

Figure 3 shows the radial, vertical and toroidal components of the magnetic force. Figure 3(a) indicates that the radial component opposes the accretion of matter onto the central object. Figure 3(b) and (c) reveals that the disk matter undergoes vertical pinching and azimuthal braking of magnetic origin. These effects became more pronounced as the magnetization increases, providing clear support for our interpretation of the results in Figure 1. Above the disk, at the transition between the resistive and ideal MHD regimes, the components F_z and F_θ change sign and become positive, acting as magnetic accelerators of the jet matter in both the poloidal and toroidal directions.

Figure 4 shows the spatial evolution curves of the poloidal components of the different forces acting on the matter in the disk-jet system. For $z < 1.6h$, the poloidal components of gravity and magnetic force (both negative) maintain the vertical equilibrium of the disk along with the poloidal component of the thermal pressure gradient. At the disk surface, both gravity and the poloidal magnetic force F_{mp} ($=\boldsymbol{F_m}.\frac{\boldsymbol{B_p}}{B}$) decrease and approach zero. This allows the thermal pressure gradient (positive) to push the disk matter into the jet, enabling the magnetic force to subsequently accelerate the jet in both the poloidal and azimuthal directions. To better understand the jet acceleration mechanism, Ferreira (1997) decomposed the Lorentz force into components parallel and perpendicular to the magnetic surfaces as follows:

$$F_{\parallel} = \frac{B_p}{2\pi r} \nabla_{\parallel} \quad I, \tag{18}$$

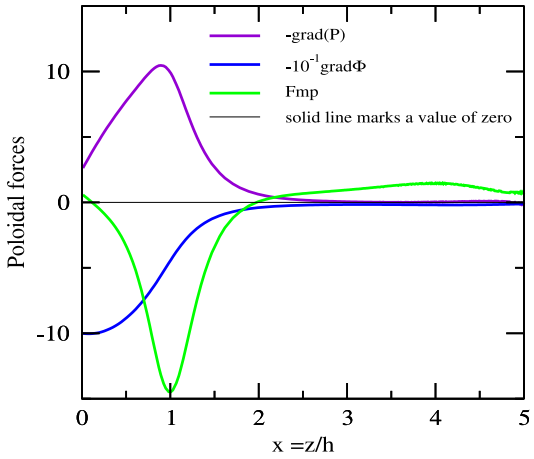


Figure 4. Spatial evolution of the poloidal components of magnetic force, gravity and pressure gradient for $\mu = 0.7$.

$$F_\theta = \frac{-B_\theta}{2\pi r} \nabla_\parallel \quad I, \tag{19}$$

$$F_\perp = B_p j_\theta - \frac{B_\theta}{2\pi r} \nabla_\perp \quad I, \tag{20}$$

where $\nabla_\parallel$ and $\nabla_\perp$ are derivatives along and perpendicular to the magnetic surfaces of the total current $I = 2\pi r B_\theta$ respectively.

Equations (18) and (19) highlight the two mechanisms of poloidal and azimuthal acceleration. The relative importance of these mechanisms has been further studied by Ferreira (1997), Zanni et al. (2007) and Tzeferacos et al. (2009) by evaluating the ratio $-B_\theta/B_p$ as a function of the magnetic diffusivity and magnetization parameters. When B_θ is greater than B_p, the acceleration is mainly poloidal, whereas when $B_\theta << B_p$, the centrifugal acceleration dominates. Regardless of the values of the magnetic diffusivity and magnetization, the works of Zanni et al. (2007) and Tzeferacos et al. (2009) have shown that magnetocentrifugal acceleration is more significant near the disk's surface. Zanni et al. (2007) demonstrated that for relatively weak magnetization, the jet acceleration is poloidal, and becomes increasingly effective as magnetic diffusivity decreases. In the work of Tzeferacos et al. (2009), centrifugal acceleration is observed below the Alfvén surface. For weak magnetization, these authors showed that the poloidal acceleration dominates the region above the Alfvén surface. However, in magnetically dominated configurations, the magnetic poloidal force becomes small compared to the toroidal one.

Figure 5 shows that for values of μ near unity, the magnetocentrifugal acceleration mechanism described by Blandford & Payne dominates the poloidal acceleration. The significance of this acceleration mechanism diminishes as μ decreases. These results show good agreement with those presented in the works of Stepanovs & Fendt (2016) and Zanni et al. (2007).

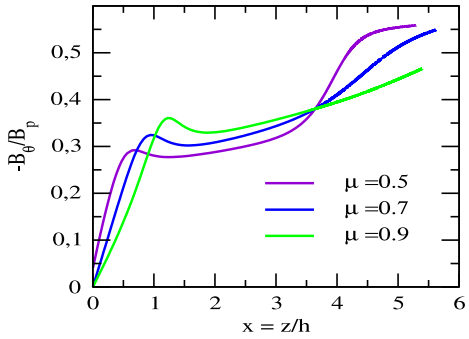


Figure 5. Spatial evolution of the ratio between the toroidal and poloidal magnetic field.

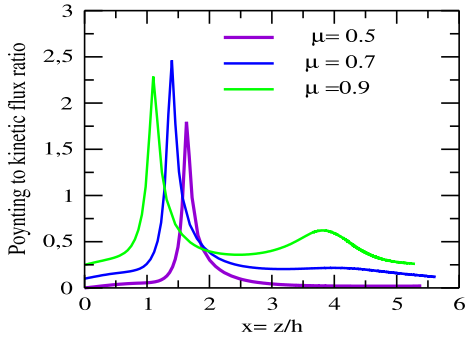


Figure 6. Spatial evolution of the Poynting flux to kinetic energy flux.

Another way to evaluate the efficiency of the acceleration mechanisms as a function of μ is by analyzing the conversion of Poynting flux into kinetic energy along a magnetic surface. This conversion is parametrized by the ratio $\sigma = -\frac{2\Omega r B_\theta B_p}{\rho u^2 u_p}$.

As shown in Figure 6, the ratio σ increases in the coronal zone of the disk as μ increases. This enhancement is primarily driven by the growth of differential rotation, which transports more magnetic energy to the jet base. Furthermore, for $\frac{z}{h} > 2$, Figure 6 shows that σ decreases with decreasing μ. This inverse relationship between σ and μ suggests that lower magnetization states correspond to reduced σ, indicating more efficient conversion of magnetic energy into kinetic energy for jet acceleration. These findings show reasonable agreement with the results of Sheikhnezami et al. (2012) and provide robust support for the validity of the results in Figure 1(b).

To examine how the magnetization parameter μ affects the jet's mass flux, we define, in Figure 7, a control volume bounded by surfaces S_i and S_e, located at $r_i = r_0$ and $r_e = 10r_0$, respectively. The top surface S_d of the control volume is set at $z = 1, 6h$, which corresponds to the height where $u_r = 0$.

The mass flux $\dot{M}_{\rm acc}(r_e)$ entering the control volume from the S_e surface and the mass flux $\dot{M}_{\rm ej}$ ejected through the S_d surface

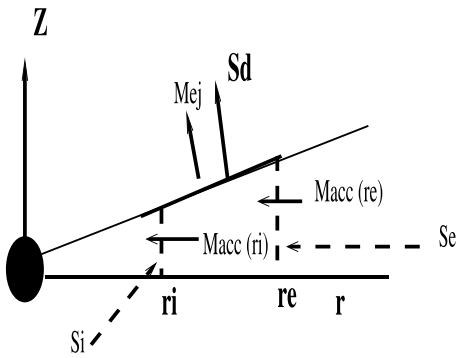


Figure 7. Control volume to measure the accretion and ejection mass flux.

Table 1
Ejection Properties

μ	0.5	0.7	0.9
$2\dot{M}_{\rm ej}/\dot{M}_{\rm acc}$	2.7%	31%	37%
$u_{p,\rm final}$	4	0.91	0.50

are calculated as follows

$$\dot{M}_{\rm acc}(r_e) = -4\pi r_e \int_0^{1.6h} \rho u_r dz,$$
$$\dot{M}_{\rm ej}(1,\, 6h) \sim 2\pi \cos(\alpha) \int_{r_i}^{r_e} \rho r u_z dr,$$

where α is the angle between $\vec{S}_d$ and the disk's rotation axis. Here, $\cos(\alpha) = \frac{1}{\sqrt{1+(1,6\epsilon)^2}}$.

The following table (Table 1) presents the ejection efficiency ($2\dot{M}_{\rm ej}/\dot{M}_{\rm acc}$) and the poloidal velocity $u_{p,\rm final}$ for three different magnetization values μ. The data reveal that increasing μ leads to higher ejection efficiency ($2\dot{M}_{\rm ej}/\dot{M}_{\rm acc}$) and lower final poloidal velocity. These results show excellent agreement with previous studies by Zanni et al. (2007) and Tzeferacos et al. (2009), indicating that jet acceleration occurs with reduced mass loading. However, this finding contrasts with the results of Stepanovs & Fendt (2016), who found that strongly magnetized accretion disks produce faster, more energetic, and less dense jets.

5. Conclusion

In this paper, we simulate a magnetized accretion-ejection disk using a stationary MHD model, where the disk, assumed to be viscous and resistive, is connected to a cold, ideal jet. In this model, the strength of the magnetic field μ is expressed as a function of the magnetic diffusivity parameter α_m through the algebraic relation: $\mu = 1/\sqrt{\alpha_m}$. Three simulation cases were considered, with μ taking the values of 0,5, 0.7 and 0.9. The obtained results are generally consistent with those in the literature and show that when the magnetic field is near equipartition with the thermal pressure in the disk midplane:

i- the vertical thermal pressure gradient is the only force capable of pushing matter from the disk surface into the jet,

ii- the jet driving mechanism follows the magneto-centrifugal Blandford & Payne scenario.

iii- efficient poloidal acceleration requires low magnetization configurations,

iv- the jet's acceleration decreases as it carries more mass.

References

Allen, A., Li, Z. Y., & Shu, F. H. 1995, ApJ, 599, 363
Anderson, J. M., Li, Z. Y., Krasnopolsky, R., & Blandford, R. 2005, ApJ, 630, 945
Blandford, R. D., & Payne, D. G. 1982, MNRAS, 199, 883
Cabrit, S., Edwards, S., & Strom, S. E. 1990, ApJ, 354, 687
Casse, F., & Ferreira, J. 2000, A&A, 353, 1115
Casse, F., & Keppens, R. 2002, ApJ, 581, 988
Casse, F., & Keppens, R. 2004, ApJ, 601, 90
Fendt, C. 2006, ApJ, 651, 272
Ferreira, J. 1997, A&A, 319, 340
Ferreira, J., & Pelletier, G. 1995, A&A, 581, 807
Hairer, E., & Wanner, G. 1996, Solving Ordinary Differential Equations II, Vol. 14 (Berlin: Springer), 382
Kato, S. X., Kudoh, T., & Shibata, K. 2002, A&A, 565, 1035
Krasnopolsky, R., Li, Z.-Y., & Blandford, R. D. 1999, ApJ, 526, 631
Mellon, R. R., & Li, Z. Y. 2008, ApJ, 681, 1356
Murphy, C., Ferreira, J., & Zanni, C. 2010, A&A, 512, A82
Ouyed, R., & Pudritz, R. E. 1997, ApJ, 482, 712
Pudritz, R. E., Rogers, C. S., & Ouyed, R. 2006, MNRAS, 365, 1131
Rezgui, G., Marzougui, H., Lili, T., Preuner, R., & Ceccobello, C. 2022, MNRAS, 514, 3925
Rezgui, G., Marzougui, H., Wooding, J., Svoboda, J., & Lili, T. 2019, ApJ, 880, 811
Shakura, N. I., & Sunyaev, R. A. 1973, A&A, 24, 337
Sheikhnezami, S., Fendt, C., Porth, O., Bhargav, V. B., & Ghanbari, J. 2012, ApJ, 757, 65
Stepanovs, D., & Fendt, C. 2014, A&A, 793, 31
Stepanovs, D., & Fendt, C. 2016, ApJ, 825, 14
Tomisaka, K. 2000, ApJ, 528, 41
Tzeferacos, P., Ferrai, A., Mignone, A., et al. 2009, MNRAS, 400, 820
Uchida, Y., & Shibata, K. 1985, PASJ, 37, 515
Ustyugova, G. V., Koldoba, A. V., Romanova, M. M., Chechetkin, V. M., & Lovelace, R. V. 1999, ApJ, 516, 221
Zanni, C., Ferrari, A., Rosner, R., Bodo, G., & Massaglia, S. 2007, A&A, 469, 811